VOL. 6, NO. 1 (March 2026) 25-40
https://jagst.utm.my

JAGST
Journal of Advanced Geospatial Science & Technology

Modelling of Submerged Targets Affected by Refraction Using Green-Wavelength Leica C10 Scanstation

Adam Luqman Putera Arman Putera, Khairulnizam M. Idris*

Geospatial Imaging and Information Research Group (G12RG), Faculty of Built Environment & Surveying, Universiti Teknologi Malaysia, 81310 UTM Johor Bharu, Johor, Malaysia

*Corresponding author: khairulnizami@utm.my

***Abstract*—**This paper presents an extensive approach into the capability of terrestrial laser scanning (TLS) operating at the 532 nm green wavelength for modelling submerged targets under varying water depths with the effects of refraction acting upon the targets. In this research, a Leica 0 C10 TLS was deployed to scan a controlled rectangular pool containing a submerged cuboid target and check markers positioned equally at depths ranging from 0 to 15 cm incrementally. The Point cloud data were processed using Leica Cyclone Register and 3DSurvey software, while a MATLAB-based algorithm to solve the refraction correction based on Snell's law was applied. Results demonstrated accountable horizontal and vertical displacements of submerged markers, which are consistent with theoretical refraction effects, averaging 2cm and 2mm for the horizontal and vertical displacement, respectively, with the presence of water depth at 3cm assessed by visual evaluation of the markers. The post-processing correction using MATLAB significantly improved the alignment precision and allowed 3D mesh models to approximate the true target dimensions more accurately, presenting the mean error vectors of 1.36m for 0, 0.34m for 0, and 0.41m for 0. This paper highlights the potential of 532 nm TLS for shallow-water 3D modelling applications and the significance of refraction correction.

Keywords— *LiDAR, Green Wavelength, Refraction, 3D Mesh & Shallow Water*

Article History: Received 6 March 2026, Accepted 12 March 2026, Published 31 March 2026

How to cite: Arman Putera, A. L. P. and M.Idris, K. M. (2026). Modelling of Submerged Targets Affected by Refraction Using Green-Wavelength Leica C10 Scanstation. Journal of Advanced Geospatial Science and Technology. 6(1), 25-40. https://doi.org/10.11113/jagst.v6n1.130

1. Introduction

Three-dimensional (3D) modelling has become an essential tool across multiple industries ranging from urban planning, reverse engineering, to maritime surveys. Laser scanning systems such as LiDAR provide high-density point clouds for accurate 3D reconstruction (0 & Ioannidis, 2023). However, most commercially used terrestrial laser scanners employ near-infrared (NIR) wavelengths, which are significantly absorbed by water, limiting their ability to model submerged objects. Recent developments have seen the introduction of green wavelength (532 nm) lasers, which are capable of penetrating shallow water, enabling terrestrial laser scanning of submerged targets. Nonetheless, the impact of refraction at the air-water interface on modelling accuracy remains insufficiently quantified, while the more well-known existing method of using sonar is well documented and utilized in the industry (Latifi et al., 2023). This study addresses this gap by evaluating the precision and capability of 532 nm TLS for modelling submerged entities under refractive conditions caused by shallow water in a controlled environment. It further highlights the importance of recognising refraction error as a factor affecting data precision, examines the general limitations of green-wavelength LiDAR, and assesses a MATLAB-based refraction correction approach using point cloud data.

1.1. Terrestrial Laser Scanning (TLS)

Point cloud data is the output of a laser scanning device. By producing laser beams and measuring the time it takes for the beams to return to the scan station, the system can estimate the target's distance from the scan station and get point cloud data. Due to the flawless redundancy of laser scanning data, this survey approach has grown increasingly common. The point cloud is guaranteed to be accurate and immersive digital copies since the laser beams that are emitted make direct contact with the targets, which increases the trust levels of users (0 et al., 2024). Either having the ability to obtain precise 3D data and estimate the parameters at the pixel scale, or by employing voxels to expand into 3D space (Maxwell et al., 2023).

A single scan position is typically insufficient to accurately represent the target in a 3D representation. Multiple scans are required to illustrate a target that is adequate in terms of standard surveying standards because the scan positions can significantly affect the findings when determining the distances between the targets. The locations of the scan stations that must be appropriately encircling the target are one of the key elements that have a greater impact on data quality. Obtaining a high point density helps compensate for low positional quality in isolated points and increases geometric precision, but failing to place the scan stations around the target optimally could make registration problematic (Alves et al., 2023).

1.2. Green Wavelength Penetrating Water

Typically, for a laser scanning system to successfully gather the set of data, the projected laser's ability to reach the target is a crucial component. In this regard, the laser type and projected light wavelength are very important aspects that will determine the reliability of the data (Janowski et al., 2022). The features of wavelengths vary gradually along the electromagnetic spectrum, which is the reason why choosing the right wavelength is essential to the success of a laser scanning project (Janowski et al., 2022). In contrast to the NIR wavelength, the majority of TLS that use NIR only obtain data on the water's surface. This occurs because NIR is greatly absorbed by the water's surface when it contacts it, resulting in the data only obtaining the point cloud for the water's surface (Janowski et al., 2022).

The green wavelength can map or simulate the submerged creatures from a different medium because it can pass through the water's surface. Green wavelengths can penetrate the sea surface to a certain degree since their rate of absorption by water is lower than that of near-infrared radiation (Janowski et al., 2022). But according to Miura & Asano (2013), who conducted a study aimed at comprehending and forecasting the movement of water and sediment in mountain channels for efficient disaster risk management, the 532 nm green wavelength seemed to be a step forward in handling the air-water interface situation because it is less absorbed by water than the NIR wavelength in terms of laser scanning. Nevertheless, a systematic inaccuracy known as the refraction error, which results in a displacement of light propagation, is unavoidable and must be addressed when data collecting involves several media, in this case, water and air (Zhang et al., 2022). Figure 1 presents the capability of the green wavelength laser to reach the ground surface and penetrate the water surface which allows and opens various possibilities in data capturing.

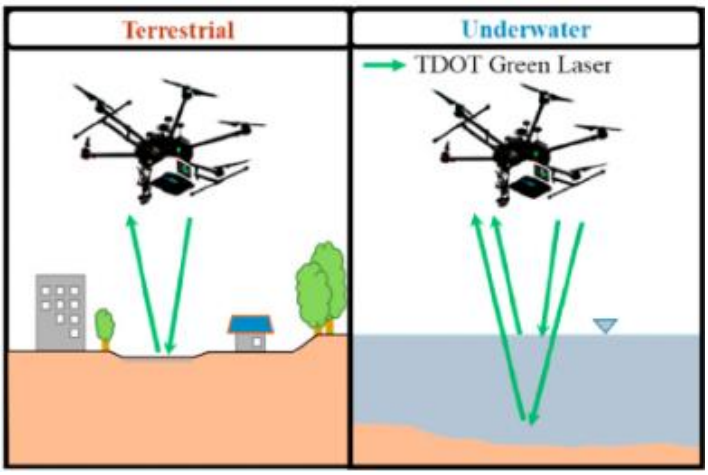

Figure 1: Green Wavelength Penetrating the Water Surface (Islam et al., 2023)

1.3. Refraction Effects and Correction

It is possible to say that light is traveling through the air, which is a solitary medium, when a light beam is released into the atmosphere. Refraction happens, for instance, when a light beam is focused into a pool of water, allowing it to travel through both air and water as a multi-medium. Refraction is the process by which a light beam changes its direction as it travels through a new medium, which often has a different refractive index (Britannica, 2023). The computed ratio of the speed of light in a vacuum to the speed of light in a second medium with a higher or lower density is known as the refractive index (Britannica, 2019).

In terms of demonstration, air and water are typically utilized as the media. The air has a refractive index of one since it is known as the vacuum mentioned previously. Since water has a slightly higher density than air, its refractive index is typically 1.33 (Britannica, 2019). It may be stated that refraction will take place when a light beam travels through air, which is a less dense medium, and then into water, which is a denser medium because of this. Light is redirected from the angle of incidence into the angle of refraction because of refraction (0, 2022).

The light beam will undergo a similar directional change but a different magnitude when it passes through any other denser media after exiting air. Equation 1 presents the Snell's law that is applied to calculate the results of refraction of a light ray through different densities. ((Jaud et al., 2025).

$$n_1 sin_{\theta 1} = n_2 sin_{\theta 2} \qquad \text{(equation 1)}$$

n_1 = Incident Index
n_2 = Refracted Index
$sin_{\theta 1}$ = Incident Angle (i)
$sin_{\theta 2}$ = Refracted Angle (r)

1.4. Water Surface Modelling and Signal Attenuation

The modelling of the water surface is crucial for any refraction correction algorithm. In this study, the water surface was approximated as a mean plane derived from averaged pulse returns. However, natural water bodies are dynamic, with waves and ripples altering the interface plane and complicating refraction correction. Another critical factor is signal attenuation. Even at the green wavelength, scattering by suspended particles and absorption by water molecules reduce signal strength with depth. At depths beyond 12–15 cm in the experiment, point density dropped sharply. These effects must be accounted for in operational surveys, where turbidity can vary dramatically.

2. Research Methodology

Figure 2 presents the flowchart of how this research project was approached and executed. Generally, the whole methodology can be split into 3 phases which 1st phase is mainly focused on background studies for the problem identified, 2nd phase's primary objective was to obtain the data properly as so in the 3rd phase, the data was discussed and analysed systematically.

A controlled experiment was conducted in a rectangular frame pool (3 m×2 m×0.75 m). The pool allowed precise control of water depth. A solid cuboid brick target (215×102×70 mm) wrapped with a checkered control-point design and five distributed check points served as references. The markers provided ground truth for displacement measurement under increasing water depths.

The Leica 0 C10 TLS, operating at 532 nm, scanned from four stations surrounding the pool at water depths of 0, 3, 6, 9, 12, and 15 cm. Each station was carefully positioned to maximize overlapping fields of view and reduce blind spots. The scan rate was up to 50,000 points per second with an angular resolution adequate to produce a dense point cloud of the submerged target.

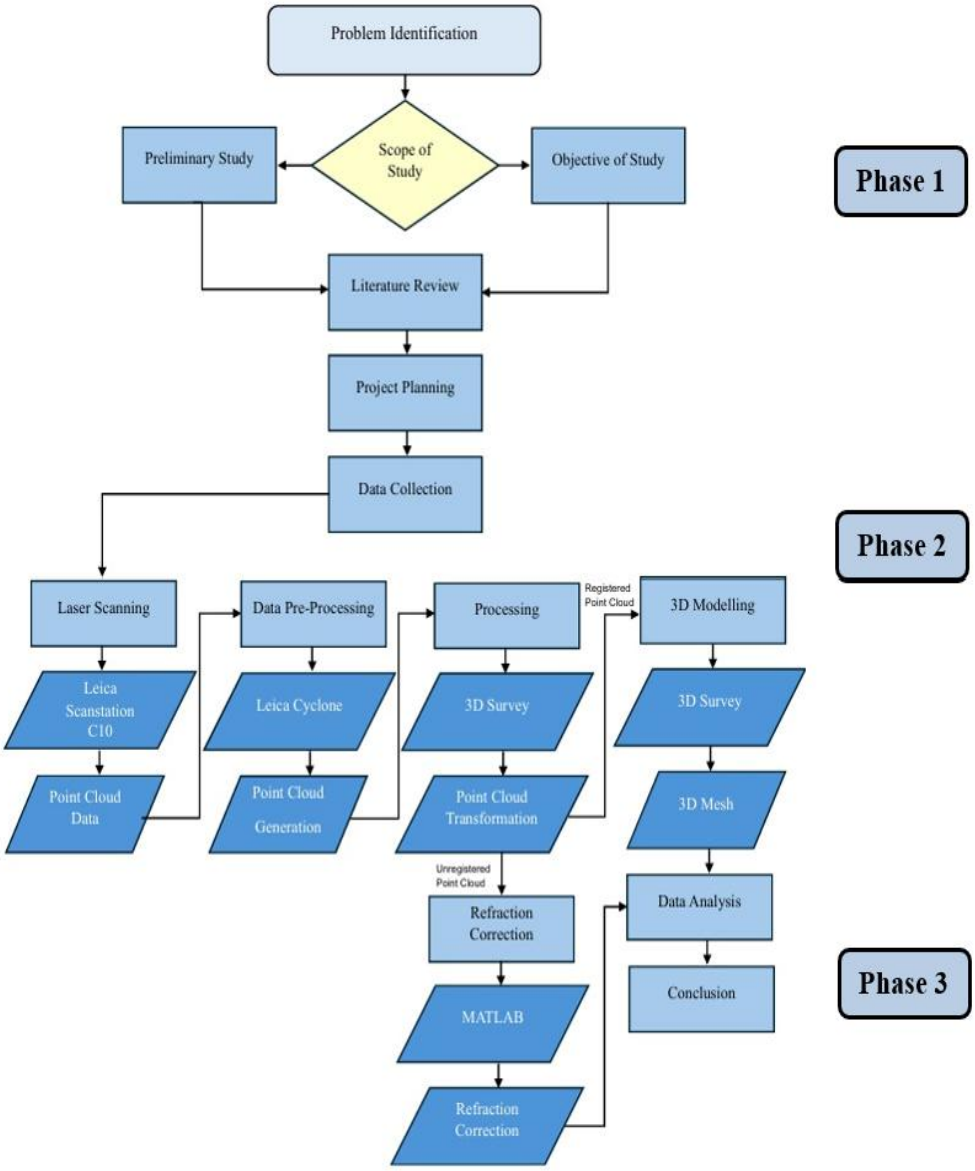

Figure 2: Methodology Flowchart

Data registration employed Leica Cyclone, using the 0 cm water dataset as a reference control. Cloud-to-cloud registration errors were computed and monitored to ensure quality. MATLAB scripts implemented Snell's law to correct for refraction: the interface plane was computed from averaged pulse returns, and correction vectors were applied to each point in the submerged point cloud.

Finally, 3DSurvey software was used to transform corrected point clouds into 3D meshes. The meshing resolution was set to closely approximate the true dimensions of the cuboid target. Metrics such as mean edge length deviation and volumetric error were computed to quantify mesh accuracy. Figure 3 presents the data acquisition layout of where the rectangular pool is placed on the floor with several control and check markers placed inside and outside of the pool

for reference. A cuboid brick is placed inside the pool used as the target for the point cloud modelling assessment.

Figure 3: Data Acquisition Layout

3. Results and Discussion

The results are discussed and expanded upon the pre-processing and point cloud transformation, visual assessment of refraction effects, quantitative analysis of marker coordinates, refraction correction using a MATLAB approach, and 3D mesh assessment. Each section contains the tables and figures showing displacements, correction improvements, and finally the mesh quality at various depths.

For the pre-processing and point cloud transformation procedure, Leica Cyclone software was used to import the raw scans captured from four scan stations. The 3 cm dataset registered correctly, but it was unable to produce an error report, most likely because of refraction-induced misalignment; meanwhile, the control dataset registered with a cloud-to-cloud error of 0.004 m. It was necessary to do a transformation process on the point cloud data, following the pre-processing step, since Leica Cyclone software does not align different datasets into one. Figure 4 shows the translation process between the control dataset and the 3cm water level data set.

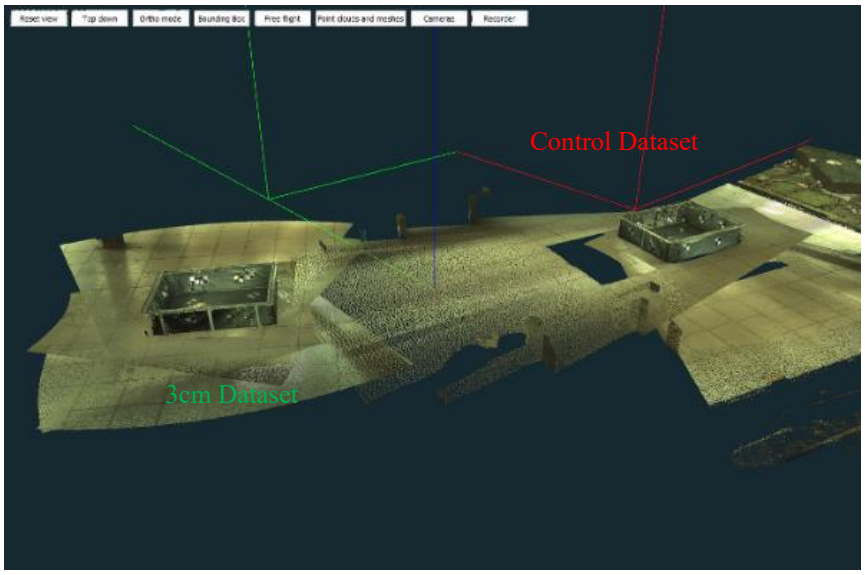

Figure 4: Point Cloud Translation between Control Dataset & 3cm Water Dataset

Some of the procedures done to ensure alignment of the datasets were to translate the datasets into a common coordinate system, according to the vector units of ΔX, ΔY, and ΔZ, the datasets were shifted to a common origin by employing obvious and observable shared reference points from the point cloud. Achieving this allows correcting orientation by yawing the CAD-calculated data in kappa units. Comparative analysis was made possible by ensuring that the control and water datasets were in alignment.

Regarding the next step of analysis (i.e. visual assessment of refraction effects), both the 3 cm water dataset and the control dataset (0 cm water) displayed distinct visible displacement of submerged markers when both datasets were superimposed. Higher incidence angles caused the edge markers to show larger shifts, but lower incidence angles caused the central marker to show smaller shifts. As predicted theoretically by Snell's law, the displacements seemed to rise linearly with water depth.

For the quantitative analysis of marker coordinates, the horizontal and vertical displacements were identified as the calculated vectors between the shift of the data and the effects of refraction. 3 common check markers were chosen from both the control and the 3 cm water dataset and used for assessment.

The horizontal displacement was calculated using equation 2 (Lam, 2024):

$$\Delta xy = \sqrt{(x_{depth} - x_0)^2 + (y_{depth} - y_0)^2} \qquad \text{(equation 2)}$$

The vertical displacement was calculated using equation 3 (Shentu et al., 2011):

$$\Delta z = z_{depth} - z_0 \qquad \text{(equation 3)}$$

To determine the vector shift of the point cloud from the effects of refraction, the visual assessment is first done by identifying 3 identifiable check markers from the control set data and from the varying, 3cm water level data. The markers are identified by the difference in colour of the marker with the rest of the floor of the rectangular pool. The coordinates of the markers from the control set data is displayed in Table 1 while the vertical difference of the coordinates of the control set data markers with the 3cm water level is shown in Table 2.

Table 1: Horizontal Displacement (0) of markers at 3 cm water level

Marker ID	x (3 cm)	y (3 cm)	Δxy (m)
CM1	999.9090	996.8570	0.023345
CM2	999.5990	997.1620	0.014318
CM3	999.2300	996.9630	0.019647

Table 2: Vertical displacement (0) of markers at 3 cm water level

Marker ID	Δz (m)
CM1	0.0010
CM2	0.0000
CM3	-0.007

To visualize the conditions of the point cloud from the control and the 3cm data set, Figure 5 shows the check markers from the control dataset while Figure 6 shows the check markers from the 3cm water level dataset.

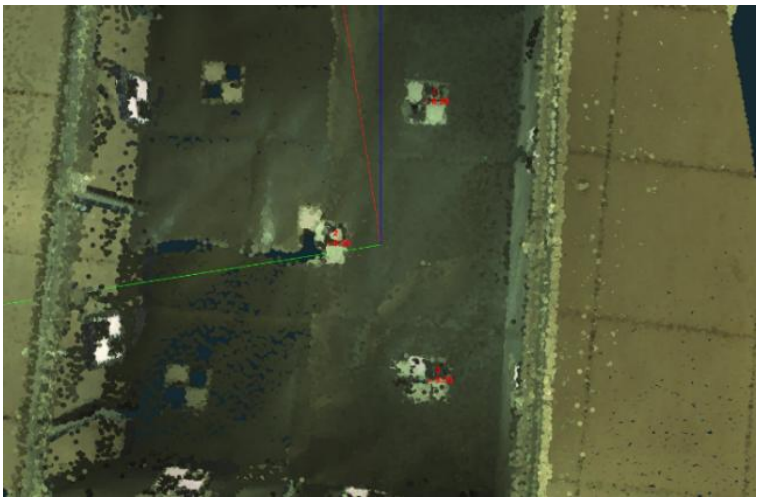

Figure 5: Control Dataset Point Cloud Highlighting the Location of Check Markers

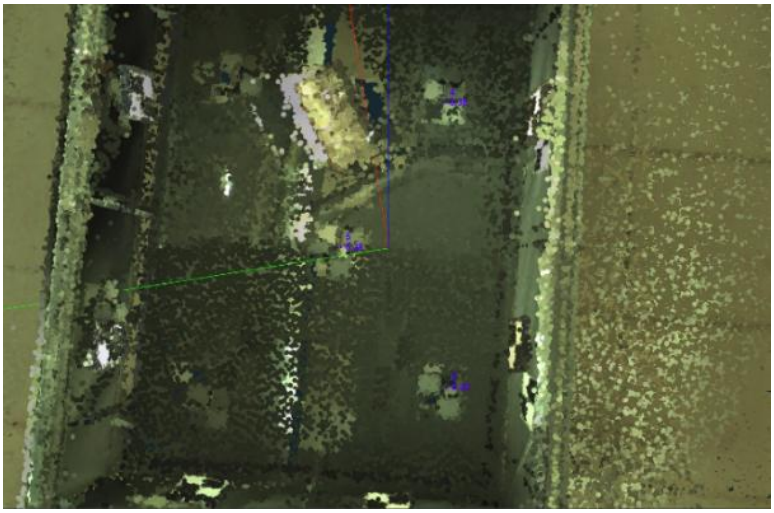

Figure 6: A 3 cm Water Level Dataset Point Cloud Highlighting the Location of Check Markers

For the refraction correction using MATLAB, this study modelled and minimized refraction at a water level of 3 cm using a correction technique. The angular displacement of the incident laser rays, the interface plane, which represents the mean water surface, and the water's refractive index (n = 1.33), were all considered throughout the correction procedure.

To analyse the resulting refraction errors on the point cloud data, the error is identified and corrected using MATLAB. 3 check markers were chosen as the sample markers to apply the refraction correction is shown in Table 3, the corrected coordinates of the check markers after applying the refraction correction is displayed in Table 4 while the amount of refraction correction for each of the check markers is shown in Table 5.

Table 3: Coordinates three sample points captured at a water depth of 3 cm with refraction

Point	x(m)	y(m)	z(m)
P1	3.358	-0.584	-1.613
P2	3.255	-1.066	-1.615
P3	2.949	-0.770	-1.618

Table 4: Coordinates of three sample points captured at a water depth of 3 cm after refraction correction are applied

Point	x Shift (m)	y Shift (m)	z Shift (m)
P1	1.9291	-0.33549	-2.0678
P2	1.8699	-0.61238	-2.0752
P3	1.6933	-0.44213	-1.9316

Table 5: Summarizes resulting refraction error vectors (0, 0, 0)

Point	0 (m)	0 (m)	0 (m)
P1	1.4289	-0.2485	0.4548
P2	1.3851	-0.4536	0.4602
P3	1.2557	-0.3279	0.3136

About the 3D mesh assessment, the datasets were classified using a two-tier classification approach, which distinguished between non-ground points that matched the submerged target and ground points that represented the environment and pool surface. This categorization allowed for the extraction of the target-specific cloud, which was subsequently modelled.

In the registered point clouds obtained at incremental water depths of 3 cm, 6 cm, 9 cm, 12 cm, and 15 cm, target clarity progressively decreased. Direct comparison of the data sets following the influence of the water level is made possible by employing the same parameters for all data sets during the classification procedure.

The cuboid target at a 3 cm water level was consistently and clearly depicted by the non-ground categorization. However, fewer valid results could be obtained as the depth grew. Edge continuity started to partially disappear, and scattered noise spots started to appear more frequently at 6 cm. The target's silhouette was faint, disordered, and asymmetrical in space by

9 cm. By 12 and 15 cm, classification revealed a sparse cloud devoid of any recognizable structure, suggesting that the laser returns from the submerged object had been nearly entirely attenuated.

The mesh reconstructions from the non-ground point sets provide a clear visual representation of the progressive decline of visibility with depth of the object. The mesh at 3 cm preserved the target's geometric integrity, including its sharp edges and flat surfaces. At 6 cm, the object was still recognizable, but distortions in the form of uneven surfaces and incomplete geometry were visible. At 9 cm, the mesh was still degrading, displaying large gaps, twisted edges, and surface irregularities. The resulting mesh was inappropriate for any reliable dimensional analysis or modelling because it disintegrated into a fragmented and incoherent structure at 12 cm and 15 cm. Figure 7 shows the steady decline of non-ground points identified of when the water level is increased while Figure 8 shows the steady decline of clarity and general shape of the cuboid target of when the water level is increased accordingly.

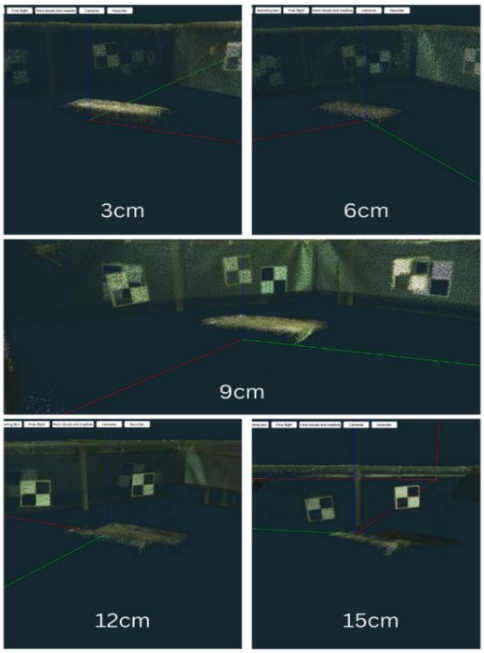

Figure 7: Decline of the density of the non-ground point cloud class centring the submerged target from a similar perspective

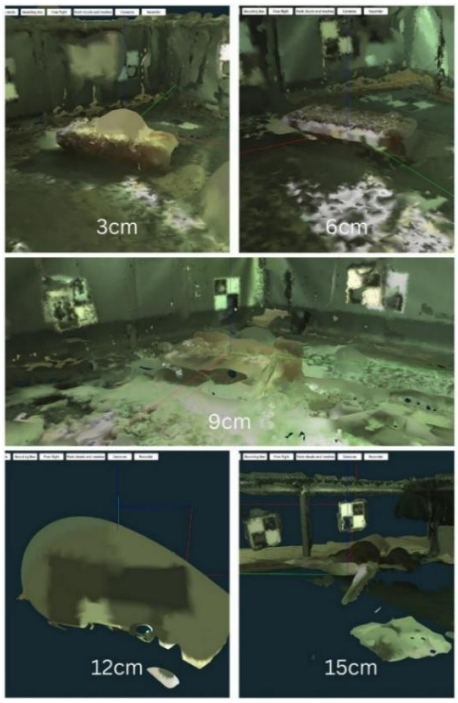

Figure 8: Decline of shape on the 3D mesh centering the submerged target from a similar perspective

This study confirms that TLS operating at 532 nm can model submerged entities in shallow water, though refraction introduces systematic displacement that must be corrected. The proposed MATLAB refraction correction approach effectively reduced displacement and improved 3D modelling accuracy. Beyond quantitative results, practical considerations include critical placement of scan stations for high point cloud density and the observation that backscatter and signal attenuation increased with depth, reducing point density at 12 cm and 15 cm depths. Future work should examine greater depths, varying turbidity, and dynamic water surfaces to expand the applicability of green-wavelength TLS for hydrographic and engineering surveys.

4. Conclusion

The findings of this research project indicates that the green wavelength at 532 nm has the potential and the capability to effectively capture and simulate submerged objects to a certain level. This capability is the result upon the use of appropriate parameters and controlled conditions, as detailed in the analysis. By carefully optimizing these factors, the green wavelength can provide considerate data for underwater imaging and object detection, demonstrating its practical applicability in relevant fields.

However, an essential aspect that cannot be overlooked is the necessity to conduct the refraction corrections. When light passes from one medium to another that possesses different densities, such as from air to water, conceptually according to Snell's law, the light ray bends due to differences in refractive indices. This bending can manipulate the captured data, leading to inaccuracies in the representation of submerged objects. The study emphasizes that without properly addressing these refraction effects, the reliability of the measurements is compromised, which can undermine the overall effectiveness of the imaging process.

Furthermore, the importance of refraction corrections becomes even more critical in industrial applications where precision is essential. The results of this research highlight that neglecting to apply these corrections can significantly degrade the accuracy of the data obtained, potentially leading to errors in measurements and flawed outputs.

Acknowledgment

The author expresses utmost gratitude to Teknologi Malaysia's (UTM) Faculty of Built Environment and Surveying and UTM Encouragement Research (UTMER) Grant (Q.J130000.3852.31J94) for the financial and technical support received throughout this research.

Conflicts of Interest

The author declares that there is no conflict of interest regarding the publication of this paper.

References

Alves, S. D., Rodríguez, F. A., Sampaio, L. F., De Medeiros, L. Í., Wiggers, D., Veiga, L. A., & Klein, I. (2023). A new approach for structural monitoring based on terrestrial laser scan data using control planes. Anuário Do Instituto de Geociências, 46. https://doi.org/10.11137/1982-3908_2023_46_53598

Britannica, T. E. of E. (2019, December 23). Refractive index. Encyclopædia Britannica. https://www.britannica.com/science/refractive-index

Britannica, T. E. of E. (2023, March 23). Refraction. Encyclopædia

Hinaniya, D. (2022, August 23). Refraction of light - definition, types, laws, effects, and examples. GeeksforGeeks. https://www.geeksforgeeks.org/refraction-of-light/

Islam, M. T., Yoshida, K., Nishiyama, S., & Sakai, K. (2023). Mutual validation of remote hydraulic estimates and flow model simulations using UAV-borne lidar and deep

learning-based imaging techniques. Results in Engineering, 20, 101415. https://doi.org/10.1016/j.rineng.2023.101415

Janowski, L., Wroblewski, R., Rucinska, M., Kubowicz-Grajewska, A., & Tysiac, P. (2022a). Automatic classification and mapping of the Seabed Using Airborne Lidar bathymetry. Engineering Geology, 301, 106615. https://doi.org/10.1016/j.enggeo.2022.106615

Janowski, L., Wroblewski, R., Rucinska, M., Kubowicz-Grajewska, A., & Tysiac, P. (2022b). Automatic classification and mapping of the Seabed Using Airborne Lidar bathymetry. Engineering Geology, 301, 106615. https://doi.org/10.1016/j.enggeo.2022.106615

Jaud, M., Geindre, M., Bertin, S., Benoit, Y., Cordier, E., Floc'h, F., Augereau, E., & Martins, K. (2025, November 27). Correction of refraction effects on unmanned aerial vehicle structure-from-motion bathymetric survey for Coral Reef Roughness Characterisation. MDPI. https://doi.org/10.3390/rs17233846

Konstantakis, M., Trichopoulos, G., Aliprantis, J., Gavogiannis, N., Karagianni, A., Parthenios, P., Serraos, K., & Caridakis, G. (2024). An improved approach for generating digital twins of cultural spaces through the integration of photogrammetry and Laser Scanning Technologies. Digital, 4(1), 215–231. https://doi.org/10.3390/digital4010011

Lam, T. Q. K. (2024, January 19). Horizontal displacement at the top of the building with frame and shear walls structures according to TCVN 2737:2023. Multidisciplinary Science Journal. https://dx.doi.org/10.31893/multiscience.2024121

Latifi, H., Valbuena, R., & Silva, C. A. (2023). Towards complex applications of active remote sensing for ecology and conservation. Methods in Ecology and Evolution, 14(7), 1578–1586. https://doi.org/10.1111/2041-210x.14154

Maxwell, A. E., Gallagher, M. R., Minicuci, N., Bester, M. S., Loudermilk, E. L., Pokswinski, S. M., & Skowronski, N. S. (2023). Impact of reference data sampling density for estimating plot-level average shrub heights using terrestrial laser scanning data. Fire, 6(3), 98. https://doi.org/10.3390/fire6030098

Miura, N., & Asano, Y. (2013). Green-wavelength terrestrial laser scanning of mountain channel. ISPRS Annals of the Photogrammetry, Remote Sensing and Spatial Information Sciences, II-5/W2, 187–192. https://doi.org/10.5194/isprsannals-ii-5-w2-187-2013

Shentu, N., Zhang, H., Li, Q., Zhou, H., Tong, R., & Li, X. (2011, December 28). A theoretical model to predict both horizontal displacement and vertical displacement for

electromagnetic induction-based deep displacement sensors. MDPI. https://dx.doi.org/10.3390/s120100233

Verykokou, S., & Ioannidis, C. (2023). An overview on image-based and scanner-based 3D Modeling Technologies. Sensors, 23(2), 596. https://doi.org/10.3390/s23020596

Zhang, D., Chen, Y., Le, Y., Dong, Y., Dai, G., & Wang, L. (2022). Refraction and coordinate correction with the JONSWAP model for icesat-2 bathymetry. ISPRS Journal of Photogrammetry and Remote Sensing, 186, 285–300. https://doi.org/10.1016/j.isprsjprs.2022.02.020